

Molecular Docking and Molecular Dynamic Investigations of Xanthone-Chalcone Derivatives against Epidermal Growth Factor Receptor for Preliminary Discovery of Novel Anticancer Agent

Yehezkiel Steven Kurniawan¹, Ervan Yudha¹, Gerry Nugraha², Nela Fatmasari¹, Harno Dwi Pranowo¹, Jumina Jumina^{1*}, and Eti Nurwening Sholikhah³

¹Department of Chemistry, Faculty of Mathematics and Natural Sciences, Universitas Gadjah Mada, Sekip Utara, Yogyakarta 55281, Indonesia

²Pharmacy, STIKES 'Aisyiyah, Jl. Kol. H. Burlian No. 32 A, Palembang 30961, Indonesia

³Department of Pharmacology and Therapy, Faculty of Medicine, Public Health and Nursing, Universitas Gadjah Mada, Yogyakarta 55281, Indonesia

* **Corresponding author:**

email: jumina@ugm.ac.id

Received: August 29, 2023

Accepted: November 9, 2023

DOI: 10.22146/ijc.88449

Abstract: Epidermal growth factor receptor (EGFR) is found to be overexpressed in cancer cells as it controls angiogenesis, cell signaling, and proliferation mechanisms. Therefore, EGFR has been known as a common target for the initial screening of new anticancer agents. Either xanthone or chalcone has been evaluated as the anticancer agents, and their activity strongly depends on the type and position of the attached functional group. Therefore, molecular hybridization between xanthone and chalcone could yield novel anticancer agents through the EGFR inhibition mechanism. Herein, a series of xanthone-chalcone derivatives with hydrogen-bond-acceptor or hydrogen-bond-donor substituents at ortho, meta, and para positions was evaluated as the EGFR inhibitor. Thirty-seven xanthone-chalcones were designed and docked in the active site of EGFR. Compared to the native ligand, pristine xanthone-chalcone gave a 1.215× stronger binding energy and a 13.97× lower binding constant. Compound 3SH was found to be the most promising candidate due to its strongest binding energy (−9.71 kcal/mol) and the lowest binding constant (0.08 μM). Furthermore, molecular dynamic studies demonstrated that complex EGFR-3SH was stable for 100 ns simulation. These *in silico* investigations show that the xanthone-chalcone derivative is a promising novel anticancer agent to be examined through *in vitro* and *in vivo* assays.

Keywords: chalcone; EGFR; molecular docking; molecular dynamics; xanthone

■ INTRODUCTION

Cancer has become the deadliest disease over the past several years. It was reported that around 15 million patients suffered from cancer in 2020. Of those patients, almost 32% of them died due to the lack of innovation in chemotherapy treatment. Unfortunately, the World Health Organization estimated that the number of cancer active cases will reach 24 million in 2030 [1-2]. Because of that, new technology in chemotherapy treatment shall be established soon. Chemotherapy is a cancer therapy employing chemical compounds as the anticancer agent.

Thousands of new chemotherapy agents have been isolated from natural sources and/or synthesized through chemical procedures [3]. However, these processes are time-consuming due to tedious and complicated experimental work. Moreover, the isolated/synthesized compounds sometimes gave unsatisfactory anticancer activities [4-5].

Computer-aided drug design offers a powerful tool to design and screen new chemotherapy agents [6-7]. In this *in silico* assay, the crystalline structure of protein receptors inside the cancer cells is modeled and simulated in the presence of a new chemotherapy agent

[8]. The generated interactions between the chemical compound and the protein receptor could be predicted, and some parameters, such as binding energy and binding constant, could be obtained [9]. A stronger binding energy and a lower inhibition constant reflect a better anticancer agent [10].

Among the protein receptors, the epidermal growth factor receptor (EGFR) is a tyrosine kinase receptor located on the surface of cancer cells. In other words, EGFR is a transmembrane protein that plays a pivotal role in angiogenesis, cell signaling, and cell proliferation mechanisms [11]. Therefore, inhibition of the EGFR receptor leads to a cellular imbalance that may cause disturbance in the differentiation, proliferation, and growth of cancer cells [12]. Overexpression of EGFR has been reported in 60% of lung cancer patients, 58% of large cell carcinoma patients, 43% of breast cancer patients, 39% of adenocarcinoma patients, 38% of squamous cell carcinoma patients, and to some extent in prostate, colon, urinary bladder, melanoma, kidney, nasopharynx, leukemia, pancreas, and thyroid cancer cells [13].

From the biochemistry point of view, the EGFR receptor consists of 992 amino acid residues with a total structural mass of 38.27 kDa [14]. In 2002, the EGFR receptor was deposited by Stamos et al. [15] with a PDB ID of 1M17. In general, the EGFR receptor is divided into four domains, i.e., two leucine-rich and two cysteine-rich domains. Both leucine-rich domains are critical for the peptide bonding sites, while the cysteine-rich domains are pivotal in the activation of EGFR. Therefore, EGFR has been well-known as one of the most targeted proteins in the early evaluation of anticancer agents [16]. Choe et al. [17] reported that EGFR protein has also been employed in the clinical trials of Tarceva® and Iressa® on non-small cell lung cancer patients. Since the three-dimensional crystal structure of EGFR has been available online in the protein databank, a computer-aided drug design can be performed to find the lead compound in anticancer drug design and development [18]. The three-dimensional chemical structure of the anticancer agents can be built and docked in the active site of EGFR protein through molecular docking studies [19].

Recently, molecular dockings have been thoroughly

investigated for the virtual screening of anticancer agents [20]. Through molecular docking studies, the best conformation of the anticancer agent can be elucidated in the active site of the EGFR receptor, and then the virtual screening will be made based on the rank of generated docking scores. However, molecular docking studies only observed a static simulation between anticancer agents and protein receptors [21]. In contrast, molecular dynamics simulation offers a further investigation to evaluate the stability of a complex structure between the selected anticancer agent and the targeted receptor under an artificial condition that is near the physiological condition of the cells [22].

Xanthone has been recognized as a novel anticancer scaffold nowadays [23-25]. The presence of hydroxy, chloro, bromo, carboxylic acid, amino, and other functional groups is able to enhance the anticancer activity of xanthenes [26-27]. As an example, 3-hydroxyxanthone gave anticancer activity with a half-maximal inhibitory activity (IC₅₀) value of 100 µM against MCF-7 and T47D cancer cells. The addition of chloro functional group significantly decreases the IC₅₀ value to 54 and 60 µM against both cancer cells, respectively. It means the chloro substituent enhanced the anticancer activity of xanthone up to 1.85× stronger [28]. On the other hand, chalcone is another anticancer candidate, in which the anticancer activity of chalcone strongly depends on the presence of the other functional groups such as fluoro, chloro, bromo, iodo, cyano, carboxylic acid, nitro, sulfonic acid, methyl, amino, hydroxy, and thiol [29-32]. As an example, chlorinated chalcones gave the IC₅₀ value in a range of 0.8–4.3 µM against MCF-7, HeLa, and WiDr cancer cells [33-34]. These reported results declare that either xanthone or chalcone derivatives are active anticancer agents.

Molecular hybridization of chalcone with other structures, such as benzimidazole and carbazole, as well as molecular hybridization of xanthone with pyran, cinnamate, and acridone carboxamides, have been reported. It was found that the hybrid compounds gave stronger anticancer and antiproliferative activities than the individual structures, revealing a synergistic effect on molecular hybridization due to multiple non-covalent

interactions that could be made with the cancer cells' receptors [35-39]. In light of the above findings, a molecular hybridization of xanthone and chalcone could yield novel anticancer agents to be developed in the future. However, a comprehensive study on the design and development of xanthone-chalcones as the EGFR inhibitor through a virtual screening has not been evaluated yet, even though it is crucial to know their anticancer activity before synthesizing them in real experimental work.

In this work, a series of xanthone-chalcone derivatives with a variation in the attached functional groups, including hydrogen-bond-acceptor (fluoro, chloro, bromo, iodo, cyano, carboxylic acid, nitro, and sulfonic acid) and hydrogen-bond-donor (methyl, amino, hydroxy, and thiol) substituents were evaluated as EGFR receptor. Their three-dimensional chemical structures were designed using Gaussian Software. Afterward, each of them was docked in the active site of EGFR protein in the same coordinate to replace *N*-(3-ethynylphenyl)-6,7-bis(2-methoxyethoxy)quinazolin-4-amine (erlotinib) as the native ligand. The top three most promising xanthone-chalcones were further investigated through molecular dynamics simulation for 100 ns to examine the complex stability.

■ EXPERIMENTAL SECTION

Materials and Instrumentations

The three-dimensional structures of xanthone-chalcone derivatives with various functional groups are shown in Table 1. The *in silico* investigations were performed in a computer with Intel®Xeon processor CPU E5-2650 v2@2.60 GHz. On the other hand, the three-dimensional structure of EGFR (PDB ID: 1M17) with its native ligand was downloaded from the protein databank (www.pdb.org). The used software in this work are Chimera 1.13.1, AutoDock4.2, DiscoveryStudio-2019, and YASARA.

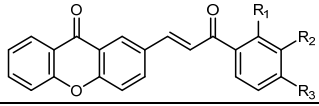
Procedure

Molecular docking of xanthone-chalcone derivatives

The chemical structures of xanthone-chalcone derivatives were built using GaussView 5.0 software and optimized in Gaussian09 software using the density

functional theory (DFT) method with Becke 3-parameters exchange potential and Lee-Yang-Parr correlation functional (B3LYP) hybrid function and 6-31G basis set.

Table 1. The three-dimensional structure of xanthone-chalcone derivatives



Entry	Molecule ID	R ₁	R ₂	R ₃
1	H	H	H	H
2	2F	F	H	H
3	3F	H	F	H
4	4F	H	H	F
5	2Cl	Cl	H	H
6	3Cl	H	Cl	H
7	4Cl	H	H	Cl
8	2Br	Br	H	H
9	3Br	H	Br	H
10	4Br	H	H	Br
11	2I	I	H	H
12	3I	H	I	H
13	4I	H	H	I
14	2CN	CN	H	H
15	3CN	H	CN	H
16	4CN	H	H	CN
17	2CO ₂ H	CO ₂ H	H	H
18	3CO ₂ H	H	CO ₂ H	H
19	4CO ₂ H	H	H	CO ₂ H
20	2NO ₂	NO ₂	H	H
21	3NO ₂	H	NO ₂	H
22	4NO ₂	H	H	NO ₂
23	2SO ₃ H	SO ₃ H	H	H
24	3SO ₃ H	H	SO ₃ H	H
25	4SO ₃ H	H	H	SO ₃ H
26	2CH ₃	CH ₃	H	H
27	3CH ₃	H	CH ₃	H
28	4CH ₃	H	H	CH ₃
29	2NH ₂	NH ₂	H	H
30	3NH ₂	H	NH ₂	H
31	4NH ₂	H	H	NH ₂
32	2OH	OH	H	H
33	3OH	H	OH	H
34	4OH	H	H	OH
35	2SH	SH	H	H
36	3SH	H	SH	H
37	4SH	H	H	SH

Afterward, the optimized chemical structures were saved in pdb format. The molecular docking protocol in this study followed the reported procedure in our previous work with slight modifications [40]. At first, the structure of EGFR and its native ligand were separated using Chimera 1.13.1 software. The water molecules were also removed from the EGFR receptor. Then, the structures of EGFR and its native ligand were prepared by adding the hydrogen atoms and Kollman charges. The re-docking studies were performed using the prepared EGFR and its native ligand within a $50 \times 50 \times 50$ Å grid box with a spacing of 0.375 Å for 100 Lamarckian genetic algorithm runnings using AutoDock4.2 software. In this docking process, the EGFR's structure was fixed, while the native ligand was set in a flexible form. The re-docking process was confirmed to be valid if the root-mean-square deviation (RMSD) value did not exceed 2.00 Å. The molecular docking studies were carried out by using similar parameters to the re-docking investigation. The xanthone-chalcone derivative was placed in the same position as the native ligand in a $50 \times 50 \times 50$ Å grid box. Then, the molecular docking results were analyzed and visualized using DiscoveryStudio-2019 software to observe interactions with amino acid residues in the active site of the EGFR receptor.

Molecular dynamics of xanthone-chalcone derivatives

The molecular dynamics of the xanthone-chalcone were carried out using YASARA software by employing the `md_runmembrane.mcr` script. The molecular dynamics simulations were conducted using several force fields, i.e., AMBER14 for the EGFR receptor, GAFF2 and AM1BCC for the ligand, and TIP3P for water molecules. The $100 \times 100 \times 100$ Å simulation box was set with a temperature of 310 K and pressure at 1 atm (NPT ensemble) with pH 7.4 and 0.9% NaCl to simulate the condition of the physiological solution. The system was minimized using the steepest descent method followed by simulated annealing minimization to obtain the desired density of 0.999 g/mL. The system was equilibrated within 250 ps at the start of the simulation to stabilize the system. The simulations were conducted for 100 ns with timesteps of 2.5 fs. The simulation snapshots were stored to the trajectories in 100 ps intervals. The cut-off value for van

der Waals forces was fixed at 8 Å, while no cut-off value was set for other electrostatic forces using the Particle Mesh Ewald algorithm. The first 5 ns solute RMSD values were assumed for equilibration time, and thus, they were excluded from Δ RMSD analysis. The molecular dynamics results, i.e., docked and molecular mechanics Poisson-Boltzmann surface area (MM-PBSA) binding energy, Δ RMSD, radius of gyration (RoG), root-mean-square fluctuation (RMSF), and solvent accessible surface area (SASA) were analyzed from each snapshot using `mcr` files.

■ RESULTS AND DISCUSSION

Molecular Docking of Xanthone-Chalcone Derivatives

In this work, we investigated a combined structure of xanthone and chalcone because both skeletons showed remarkable anticancer activities [23,32]. Thirty-seven xanthone-chalcone derivatives have been designed (Table 1). The non-substituted xanthone-chalcone (compound H) was considered as the control because this compound contains no additional functional group.

The re-docking process is conducted to evaluate the validity of the docking protocols. In the re-docking process, the native ligand was docked in the active site of the EGFR receptor. During this process, the conformation of the native ligand shall not be significantly different from the initial conformation because the initial conformation has been proved as the most stable conformation through the experimental data [21]. The superimposed structures of the native ligand in the active site of EGFR are shown in Fig. S1. Fig. S1 shows that there is no significant change between the initial conformation and the final conformation after the re-docking process. The RMSD value of the re-docking process was found to be 1.64 Å. This RMSD value is acceptable because it is less than 2.00 Å, as required in the re-docking process [41].

Fig. S2(a) and S2(b) show the location of the native ligand with the whole and active site of the EGFR receptor from the hydrogen bonds donor and acceptor point of view. The native ligand is bound with amino

acid residues of the EGFR through non-covalent interactions, as shown in Fig. S2(c). The native ligand interacted with Met769 and Cys773 amino acid residues through hydrogen bonds with a distance of 3.90 and 3.33 Å, respectively. The native ligand also interacted with Gln767, Met769, Pro770, and Gly772 residues through carbon-hydrogen bonds with a distance of 6.11, 6.82, 4.42, and 3.29 Å. The interaction between the native ligand and Leu820 was also found through pi-sigma interaction with a distance of 3.64 Å. Meanwhile, the alkyl and pi-alkyl interactions were observed between the native ligand with Leu694, Ala719, Lys721, and Leu764 residues with a distance of 5.06, 3.75, 4.30, and 4.27 Å. The native ligand was also interacted with Val702, Lys704, Glu738, Ile765, Thr766, Leu768, Asp776, Thr830, and Asp831 residues through van der Waals interactions. These non-covalent interactions led to a binding energy of -7.30 kcal/mol with a binding constant of 4.47 μ M.

The molecular docking studies in this work show the RMSD values less than 2.00 Å for all 37 compounds, demonstrating the validity of the data (Table 2). On the other hand, Fig. 1(a) and 1(b) show the location of compound H with the whole and active site of the EGFR receptor. Compound H interacted through its chalcone's carbonyl and oxygen ether of xanthone with Met769 and Lys721 residues through hydrogen bonds with a distance of 4.15 and 4.14 Å, respectively. These hydrogen bonds support our hypothesis that the hybrid xanthone-chalcone is a new promising anticancer agent because both structures could bind with the amino acid residues of the EGFR receptor. Additionally, the pi-alkyl interactions between the aromatic ring of chalcone with Leu694 (5.10 Å) and Leu768 (5.19 Å), as well as the pi-alkyl interactions between aromatic and pyran rings of xanthone with Val702 (4.84 and 6.12 Å) and Lys721 (5.71 and 6.33 Å) strengthened our hypothesis. Compound H also interacted with Phe699 and Met769 residues through pi-pi and amide-pi stacked interactions through the aromatics and pyran rings with a distance of 4.89 , 5.45 , and 5.83 Å (Fig. 1(c)), respectively. The pi-anion interactions between Asp831 residue and three six-membered rings of xanthone were observed in the active site of EGFR with a distance of 6.06 , 6.49 , and 6.52 Å.

Furthermore, the interactions between compound H and Ala719, Pro770, Gly772, and Leu820 residues were also observed through van der Waals interactions.

Table 2. The molecular docking results of xanthone-chalcone derivatives in the active site of EGFR receptor

Molecule ID	Binding energy (kcal/mol)	Binding constant (μ M)	RMSD (Å)
3SH	-9.71	0.08	0.12
3CH ₃	-9.70	0.08	0.34
2I	-9.70	0.08	0.39
2CN	-9.66	0.08	0.76
3OH	-9.51	0.11	0.32
3Cl	-9.47	0.12	1.14
3NO ₂	-9.41	0.13	1.29
2CH ₃	-9.32	0.15	0.13
4NO ₂	-9.21	0.18	0.38
2Cl	-9.17	0.19	0.21
4CH ₃	-9.02	0.24	0.09
2F	-9.00	0.25	0.82
3CO ₂ H	-8.97	0.27	1.00
H	-8.87	0.32	0.28
3I	-8.86	0.32	0.16
4F	-8.85	0.35	0.21
4SO ₃ H	-8.80	0.35	0.30
2SO ₃ H	-8.79	0.36	0.66
3SO ₃ H	-8.78	0.37	0.35
4OH	-8.77	0.37	0.19
4I	-8.75	0.38	0.14
2CO ₂ H	-8.71	0.41	1.01
4Cl	-8.61	0.49	0.31
4CO ₂ H	-8.60	0.49	0.72
4Br	-8.56	0.53	0.16
2NO ₂	-8.55	0.54	1.58
2OH	-8.55	0.54	1.69
4NH ₂	-8.52	0.57	0.22
2SH	-8.43	0.66	0.27
3Br	-8.40	0.70	0.25
3CN	-8.40	0.70	0.37
2Br	-8.29	0.84	0.14
3NH ₂	-8.12	1.12	0.64
4CN	-8.09	1.17	0.57
3F	-7.98	1.41	1.25
4SH	-7.90	1.43	0.54
2NH ₂	-7.67	2.38	1.20
Native ligand	-7.30	4.47	1.64

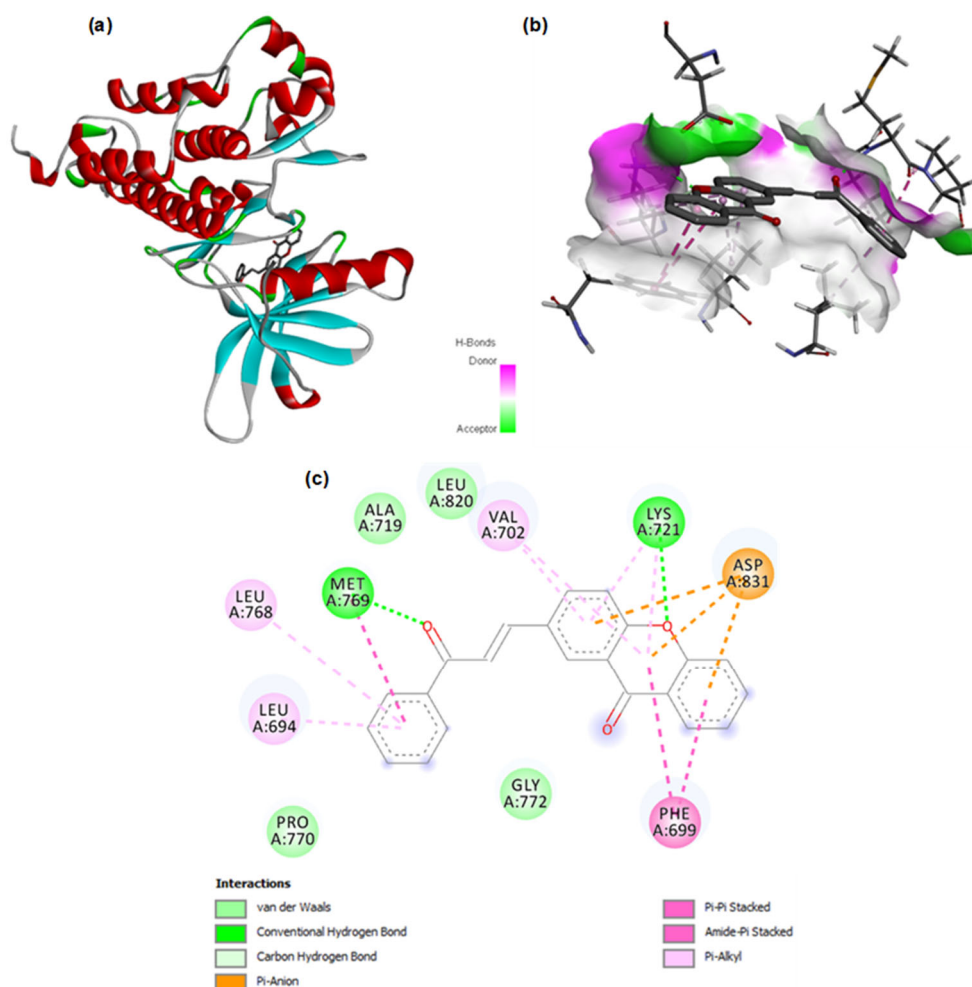


Fig 1. Molecular docking of compound H in the (a) whole structure and (b) active site of EGFR and (c) non-covalent interactions between compound H and the active site of EGFR

These interactions led to a binding energy of -8.87 kcal/mol with a binding constant of 0.32 μ M and an RMSD value of 0.28 Å. Compared to the native ligand, compound H gave a $1.215\times$ stronger binding energy and a $13.97\times$ lower binding constant than the native ligand. This result could be caused by the various non-covalent interactions of compound H (7 types of interactions) than the native ligand (6 types of interactions).

Since the pristine xanthone-chalcone showed better docking results than the native ligand, the effect of hydrogen-bond-acceptor (i.e., fluoro, chloro, bromo, iodo, cyano, carboxylic acid, nitro, and sulfonic acid substituents) and hydrogen-bond-donor (i.e., methyl, amino, hydroxy, and thiol substituents) functional groups was further investigated. Their non-covalent interactions

are shown in Fig. S3-S38, while the molecular docking results are listed in Table 2. From the investigated hydrogen-bond-acceptor groups, the order of binding energy from the strongest one to the weakest one is as follows: bromo (-8.29 to -8.56 kcal/mol) < sulfonic acid (-8.78 to -8.80 kcal/mol) < hydrogen (-8.87 kcal/mol) < carboxylic acid (-8.60 to -8.97 kcal/mol) < fluoro (-7.98 to -9.00 kcal/mol) < nitro (-8.55 to -9.41 kcal/mol) < chloro (-8.61 to -9.47 kcal/mol) < cyano (-8.09 to -9.66 kcal/mol) < iodo (-8.75 to -9.70 kcal/mol). From this order, the iodo functional group was found to be the best functional group among the other hydrogen-bond-acceptor groups. Iodo group has been known for its high anticancer agent as some approved anticancer drugs contain iodine atoms, such as iodoquinol,

diodoplatinum(IV)diamine, and trametinib [42-45]. Rappaport [46] reported that the anticancer effect of iodo group was complex and depended on the targeted cancer cells. For breast cancer cells, iodo group acts as an antioxidant agent and promotes differentiation and cell apoptosis. Meanwhile, iodo group promoted apoptosis and proliferation for endocrine carcinoma [47]. On the other hand, the molecular docking studies revealed that hydrogen-bond-acceptor group is preferable to be located at para than ortho and meta positions. This was indicated by the trend in the binding energy of para (-8.09 to -9.21 kcal/mol) > meta (-7.98 to -9.47 kcal/mol) > ortho (-8.29 to -9.70 kcal/mol) position. This order may be generated from the steric repulsion as the molecular volume for the para-substituted xanthone-chalcone was the highest of the others.

On the other side, the effect of the hydrogen-bond-donor group on the binding ability of xanthone-chalcone was also investigated in this study. Compared to the hydrogen-bond-acceptor, the hydrogen-bond-donor groups gave slightly stronger binding energy in a range of -7.67 to -9.71 kcal/mol than the hydrogen-bond-acceptor groups (-7.98 to -9.70 kcal/mol) in this work. From the investigated hydrogen-bond-donor groups, the order of binding energy from the strongest one to the weakest one is as follows: amino (-7.67 to -8.52 kcal/mol) < hydrogen (-8.87 kcal/mol) < hydroxyl (-8.55 to -9.51 kcal/mol) < methyl (-9.02 to -9.71 kcal/mol) < thiol (-8.43 to -9.71 kcal/mol). From this order, the thiol functional group was found to be the best functional group among the other hydrogen-bond-donor groups. Thiol has been known for its high anticancer agent, as some approved anticancer drugs contain sulfur and hydrogen atoms, such as mercaptopurine, 6-thioguanine, captopril, and acefylline derivatives [48-51]. It was reported that the thiol group could generate strong non-covalent interactions with the active site of the cancer cell's protein [52]. Dalzoppo et al. [53] reported that thiol-containing drugs could act as a competitive inhibitor to glutathione. Glutathione was reported to make the cancer cells become more resistant to the commercial anticancer agent. Furthermore, glutathione protects cancer cells from reactive oxygen species that are generated during photodynamic therapy.

Sun et al. [54] reported that the thiol-containing anticancer agent could generate free radicals that attack cancer cells during visible light irradiation. On the other hand, the molecular docking studies revealed that the hydrogen-bond-donor group is preferable to be located at meta than ortho and para positions. This was indicated by the trend in the binding energy of meta (-8.12 to -9.71 kcal/mol) > ortho (-7.67 to -9.32 kcal/mol) > para (-7.90 to -9.02 kcal/mol) position. This order may be attributed to suitable conformation of xanthone-chalcone derivatives in the active site of the EGFR receptor.

From Table 2, it was found that all thirty-seven xanthone-chalcone exhibit stronger binding energy (-7.67 to -9.71 kcal/mol) than native ligand (-7.30 kcal/mol) in the active site of EGFR. This result demonstrates that either binding energy or formed non-covalent interactions of xanthone-chalcone strongly depend on the type and position of hydrogen bonds donor/acceptor. All xanthone-chalcones interacted with Leu694, Val702, Leu768, and Met769 amino acid residues. Almost all xanthone-chalcones also interacted with Ala719, Lys721, Glu738, Leu764, Thr766, Pro770, Gly772, Leu820, Thr830, and Asp831 amino acid residues. The native ligand also interacted with these amino acid residues, as shown in Fig. S2(c). Furthermore, some xanthone-chalcone derivatives generated non-covalent interactions with Lys692, Phe699, Ile720, Met742, Cys751, Leu753, Phe771, Tyr777, Glu780, His781, Arg817, and Phe832 amino acid residues, which were not found in the native ligand. These interactions may explain why all xanthone-chalcones exhibit stronger binding energy (-7.67 to -9.71 kcal/mol) in the active site of EGFR than the native ligand (-7.30 kcal/mol). Table 2 also reveals that the presence of sulfonic acid, bromo, and amino was not favorable for EGFR inhibition as these compounds generate a weaker binding energy for all ortho, meta, and para positions compared to compound H. The top three best compounds were 3SH, 3CH₃, and 2I, with a binding energy of -9.71, -9.70, and -9.70 kcal/mol, respectively. These compounds gave a similar pattern for the non-covalent interactions. All of them interacted with Leu694, Val702, Ala719, Lys721,

Glu738, Met742, Leu764, Thr766, Leu768, Met769, Pro770, and Gly772 residues.

Fig. 2(a) and 2(b) show the location of the best xanthone-chalcone, i.e., compound 3SH, with the whole and active site of the EGFR receptor from hydrogen bonds donor and acceptor point of view. Compound 3SH was found to be the most promising candidate due to its strongest binding energy (-9.71 kcal/mol) and the lowest binding constant (0.08 μ M). Fig. 2(c) shows the non-covalent interactions between compound 3SH and the amino acid residues in the active site of EGFR. Compound 3SH interacted through its chalcone's carbonyl and xanthone's carbonyl with Asp831 and Met769 residues through hydrogen bonds with a distance of 2.15 and 1.83 \AA , respectively. Additionally, the thiol group at the

meta-position of the chalcone interacted with Ala719 and Thr766 through hydrogen bonds with a distance of 2.37 and 1.98 \AA , respectively. The observed hydrogen bonds in compound 3SH (4 hydrogen bonds) were higher than compound H (2 hydrogen bonds) and the native ligand (2 hydrogen bonds). This result demonstrates the key role of the thiol group at the meta-position on the enhancement of binding properties of the xanthone-chalcone framework in the active site of the EGFR receptor. Compared to compound H, the presence of thiol at meta-position gave a $1.098\times$ stronger binding energy and a $4.571\times$ lower binding constant. Meanwhile, compared to the native ligand, compound 3SH gave a $1.334\times$ stronger binding energy and a $63.86\times$ lower binding constant.

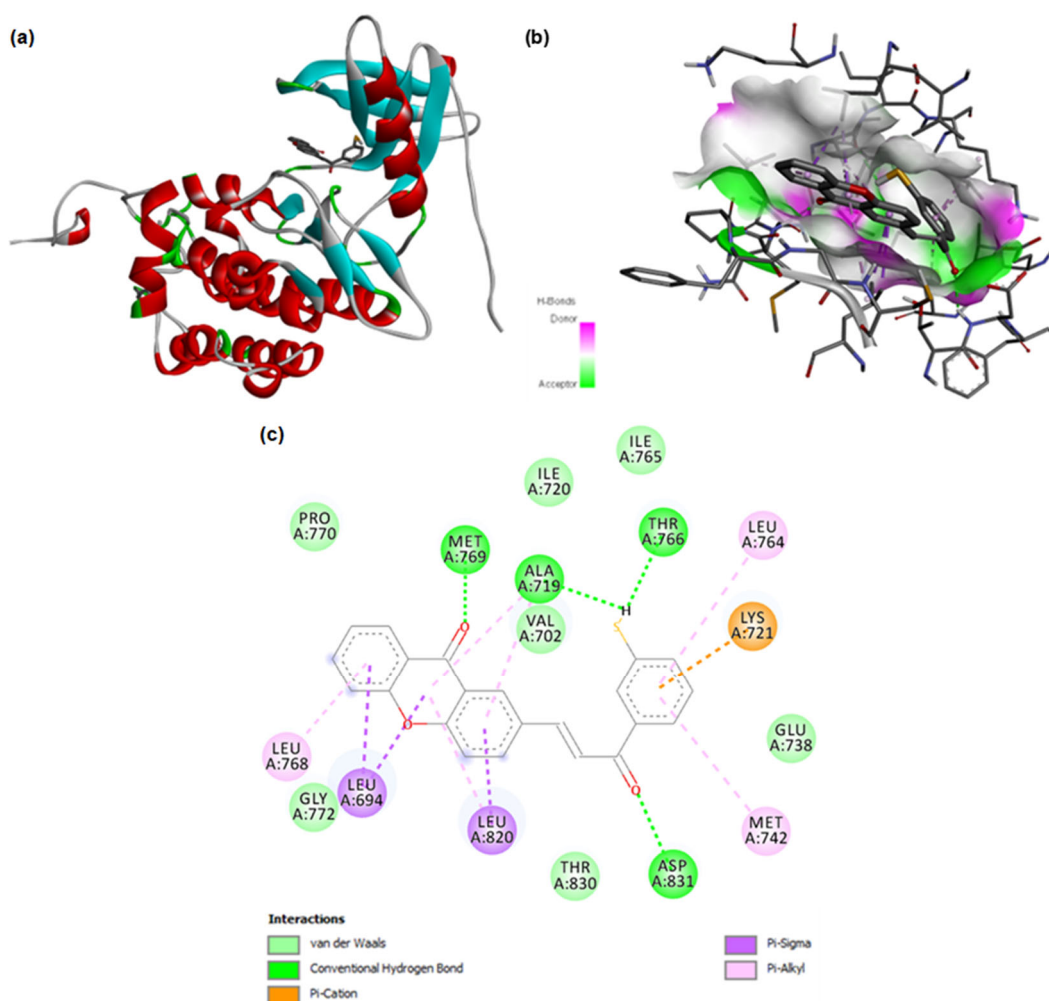


Fig 2. Molecular docking of compound 3SH in the (a) whole structure and (b) active site of EGFR and (c) non-covalent interactions between compound H and the active site of EGFR

The pi-alkyl interactions between aromatic ring of chalcone with Met742 (5.34 Å) and Leu764 (5.19 Å), as well as the pi-alkyl interactions between aromatic and pyran rings of xanthone with Ala719 (5.43 and 5.44 Å), Leu768 (5.23 Å), and Leu820 (5.30 Å) proved the good strategy for combining xanthone and chalcone structures within a hybrid compound. Compound 3SH also interacted with Leu694 and Leu820 residues through pi-sigma interactions via the aromatics and pyran rings with a distance of 3.62, 3.74, and 5.27 Å, respectively. The pi-cation interaction between Lys721 residue and aromatic ring of chalcone was observed in the active site of EGFR with a distance of 4.59 Å. Furthermore, the interactions between compound 3SH and Val702, Ile720, Glu738, Ile765, Pro770, Gly772, and Thr830 were also observed through van der Waals interactions.

It was reported that Gly695, Gly700, Ala719, Glu767, Met769, Arg812, Asp818, Asp831, Gly833, and Tyr845 play a critical role in the catalytic activity of EGFR protein, especially in the suppression of the division of cancer cells [55]. Additionally, Choowongkomon et al. [56] reported that there were five active regions in the binding pocket of EGFR receptor, i.e., sugar pocket region, phosphate binding region, adenine region, hydrophobic I and II regions. The Lys721, Glu738, and Asp831 key residues were located in the sugar pocket region near the α -helix and phosphate binding region. Meanwhile, Asp776, Glu780, and Asp831 key residues were located in the phosphate binding region along the sugar pocket region. The Val702, Met742, and Leu764 residues were reported as the key amino acid residues on the hydrophobic I region, while Leu694, Leu768, Thr766, Pro770, Phe771, and Leu820 residues were considered as the key amino acid residues on the hydrophobic region II of the EGFR receptor. These interactions were also observed in the molecular docking studies of the commercially available EGFR inhibitors, including icotinib, almonertinib, and olmutinib [57]. From the molecular docking study, compound 3SH interacted with Leu694, Val702, Lys721, Glu738, Met742, Leu764, Thr766, Met769, Pro770, Leu820, and Asp831 key amino acid residues showing a good ability of compound 3SH to disturb the function of EGFR receptor on proliferation,

angiogenesis, metastasis, and anti-apoptosis processes of the cancer cells.

Molecular Dynamics of Xanthone-Chalcone Derivatives

Further investigation was performed through molecular dynamics simulation for 100 ns to evaluate the stability of the best three complexes, i.e., EGFR-3SH, EGFR-3CH₃, and EGFR-2I, within a cube. The obtained results from the molecular dynamics simulation are shown in Fig. 3-5, respectively. The binding energy and Δ RMSD values represent the EGFR-3SH complex stability during 100 ns simulation, as shown in Fig. 3. The average docked binding energy of the EGFR-3SH, EGFR-3CH₃, and EGFR-2I complexes was -10.94, -9.48, and -4.74 kcal/mol, respectively (Fig. 3(a)). It was found that the average docked binding energy of EGFR-3CH₃ complex (-9.48 kcal/mol) during the molecular dynamic simulations was close to the molecular docking study (-9.70 kcal/mol). In contrast, compound 2I was not stable enough in the active site of EGFR because the binding energy of EGFR-2I complex was increased during the first 30 ns simulation and then reached a plateau at around -4 kcal/mol. On the other hand, the binding energy of EGFR-3SH complex was the highest among the other evaluated xanthone-chalcone complexes. Furthermore, the binding energy of EGFR-3SH complex (-10.94 kcal/mol) was close to the binding energy of EGFR-native ligand complex (-11.58 kcal/mol). On the other hand, the MM-PBSA binding energy of EGFR-3SH, EGFR-3CH₃, and EGFR-2I complexes was -43.92, +73.47, and +65.44 kcal/mol, respectively (Fig. 3(b)). All binding energy values were already equilibrated from 50 ns simulation time. The docked binding energy result agreed with the MM-PBSA binding energy value of EGFR-3SH complex, revealing that EGFR-3SH complex was the most stable complex. The MM-PBSA binding energy of EGFR-3SH (-43.92 kcal/mol) is higher than the EGFR-native ligand complex (-40.90 kcal/mol), which was remarkable. On the other hand, the average Δ RMSD value of EGFR-3SH, EGFR-3CH₃, and EGFR-2I complexes is 0.27, 0.45, and 0.45 Å, respectively (Fig. 3(c)). This result confirmed that the EGFR-3SH complex

(with the lowest average Δ RMSD value) was the most stable complex during the 100 ns simulation, agreed to the docked and MM-PBSA binding energies data.

The RMSF value of the evaluated complexes is shown in Fig. 4. The RMSF data showed a relatively stable complex structure of EGFR-3SH, EGFR-3CH₃, and

EGFR-2I with an average value of 0.19, 0.20, and 0.19 nm, respectively. On the other side, RoG and SASA values during the molecular dynamic simulation are shown in Fig. 5. The RoG graph was used to see the compactness of the protein structure from the complex, and it was found that the RoG values of the evaluated

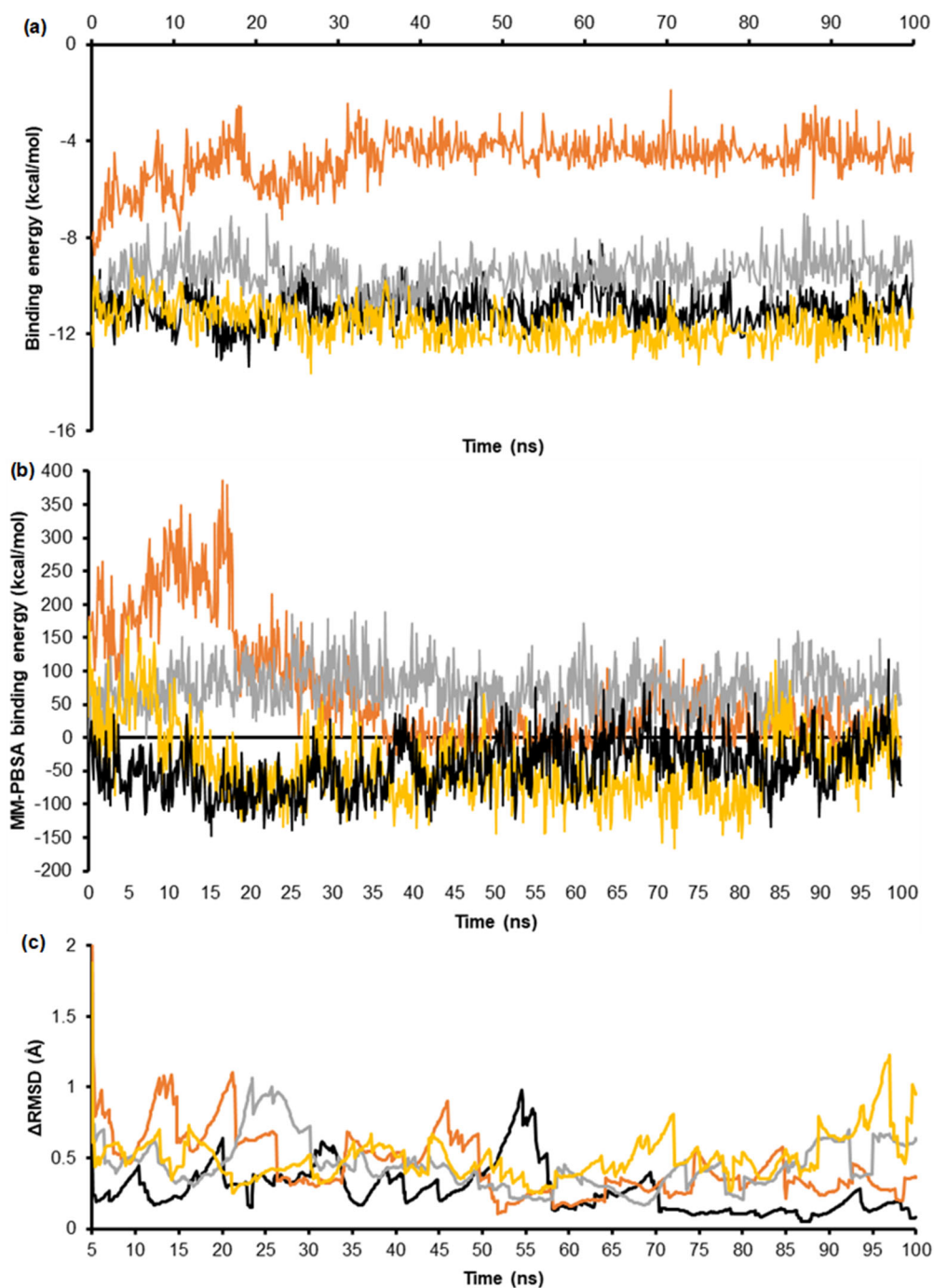


Fig 3. The (a) docked and (b) MM-PBSA binding energy and (c) Δ RMSD of EGFR-native ligand (yellow), EGFR-3SH (black), EGFR-2I (orange), and EGFR-3CH₃ (grey) complexes during the molecular dynamic simulation for 100 ns

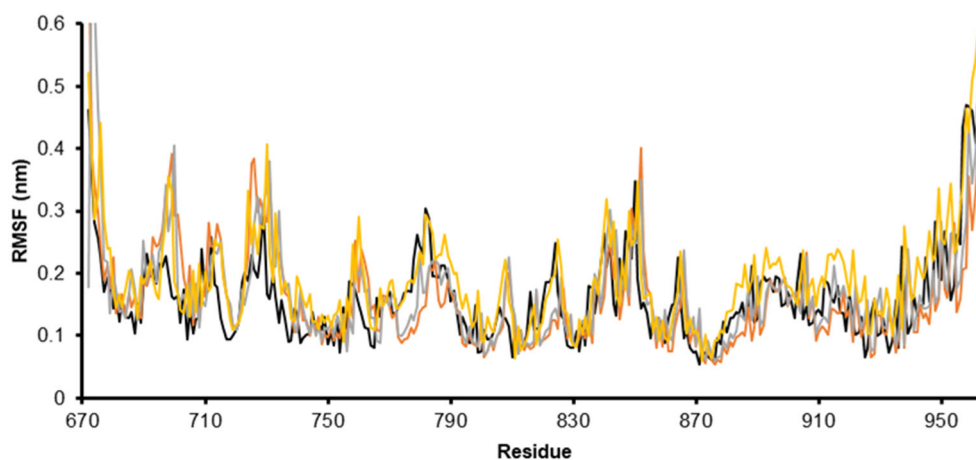


Fig 4. RMSF parameter of EGFR-native ligand (yellow), EGFR-3SH (black), EGFR-2I (orange), and EGFR-3CH₃ (grey) complexes during the molecular dynamic simulation for 100 ns

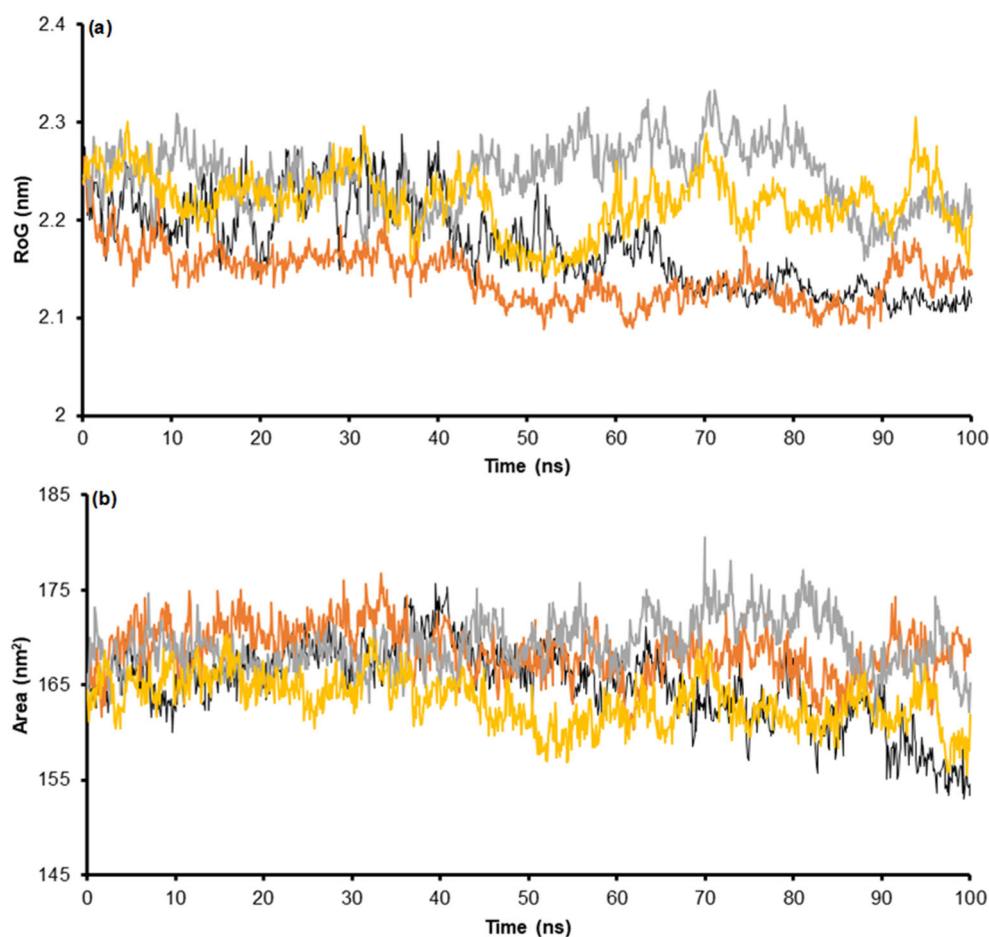


Fig 5. (a) RoG and (b) SASA values of EGFR-native ligand (yellow), EGFR-3SH (black), EGFR-2I (orange), and EGFR-3CH₃ (grey) complexes during the molecular dynamic simulation for 100 ns

three complexes varied between 2.08 and 2.33 nm. The mean RoG value of EGFR-3SH, EGFR-3CH₃, and EGFR-

2I complexes from the 100 ns simulation was 2.17, 2.14, and 2.25 nm, respectively. The SASA graph was used to

analyze the surface area of the protein that is available for water molecules to form interactions with the protein. SASA of the complex showed that the values varied from 153 to 181 nm², and the mean value for EGFR-3SH, EGFR-3CH₃, and EGFR-2I complexes was 165.10, 168.57, and 169.20 nm², respectively, from all trajectories. Thus, there was no significant change in terms of the SASA values of the complexes during the simulation. Overall, the values of both RoG and SASA values showed that the structures of EGFR-xanthone-chalcone complexes were relatively stable during the molecular dynamic simulations for 100 ns, which was in agreement with the other works [7,14,58-60].

The changes in the evaluated parameters during the molecular dynamic simulations of EGFR-3SH came from the conformational changes of the EGFR-3SH complex

(Fig. 6). At the initial point (0.00 ns), compound 3SH interacted with Leu694, Val702, Ala719, Ile720, Lys721, Glu738, Met742, Leu764, Ile765, Thr766, Leu768, Met769, Pro770, Gly772, Leu820, Thr830, and Asp831 through hydrogen bonds, pi-cation, pi-sigma, pi-alkyl and van der Waals interactions. After 100 ns simulation, a trajectory file at 95.70 ns was selected to represent the final conformation of compound 3SH in the active site of EGFR. At that time, compound 3SH still interacted with Met769 and Asp831 residues through hydrogen bonds. Other non-covalent interactions with Leu694, Val702, Ala719, Ile720, Lys721, Met742, Leu764, Ile765, Thr766, Leu768, Pro770, Gly772, Leu820, and Thr830 residues were retained. Meanwhile, new van der Waals interactions with Cys773, Arg817, and Phe832 residue were also found in the final conformation of compound

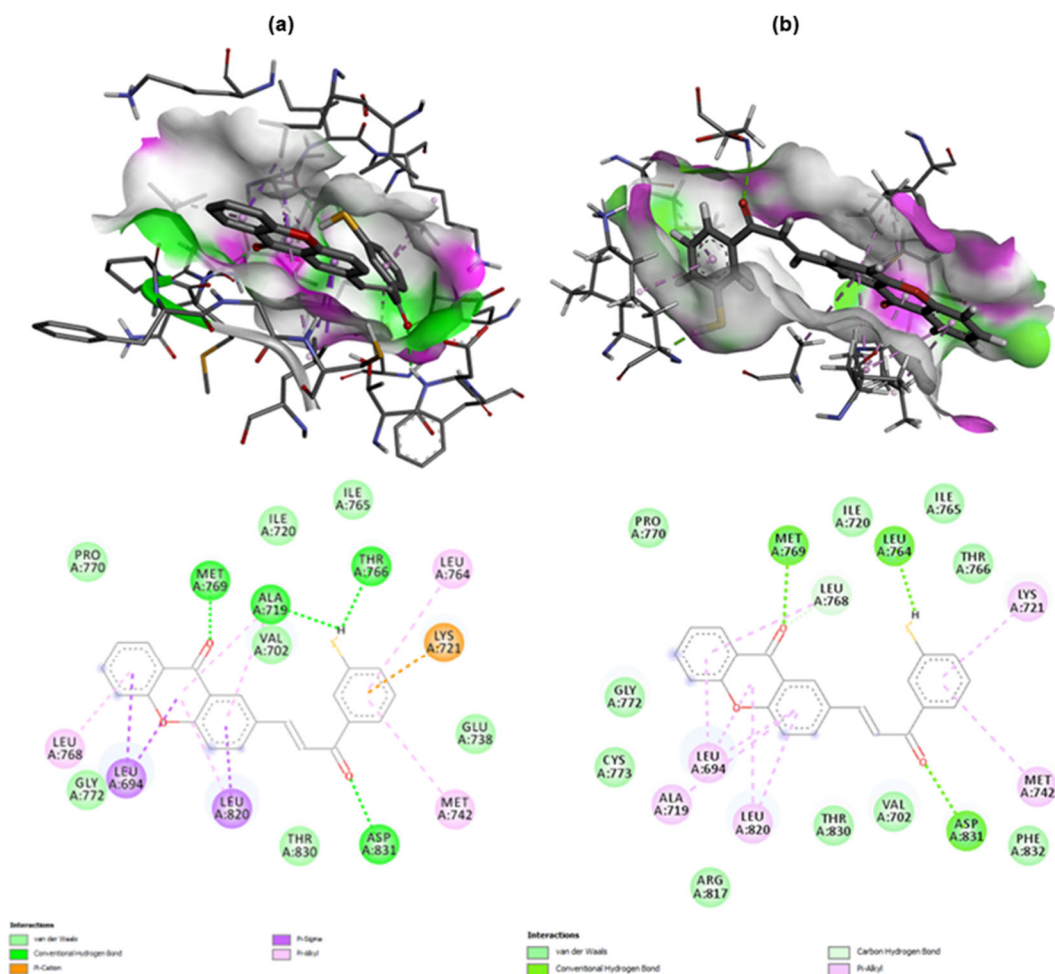


Fig 6. The observed non-covalent interactions between compound 3SH and the active site of EGFR after molecular dynamics simulation for (a) 0.00 and (b) 95.70 ns

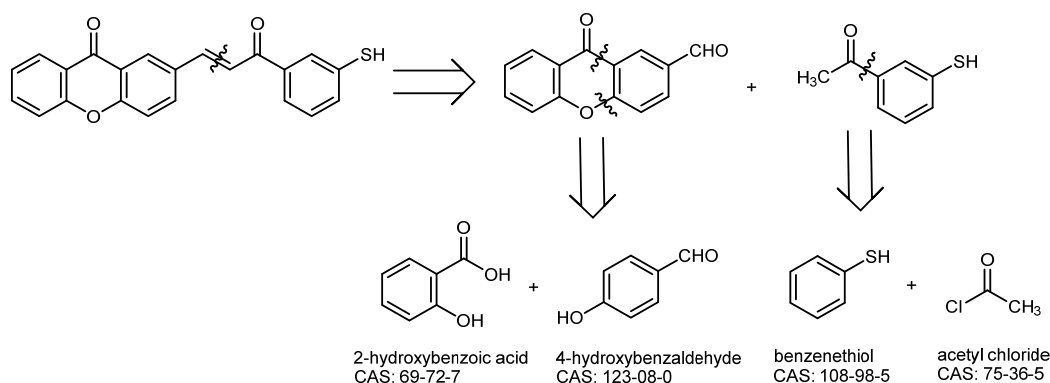


Fig 7. Retrosynthetic analysis of compound 3SH from the available raw materials

3SH in the active site of EGFR. Either the initial conformation (0.00 ns) or final conformation (95.70 ns) showed that each chalcone, xanthone, and thiol moieties interacted well with the key amino acid residues aforementioned above. These key amino acid residues are responsible for the physiological function of the EGFR receptor; thus, the observed non-covalent interactions clearly demonstrate the potency of compound 3SH as a novel anticancer agent based on the EGFR inhibition mechanism.

The retrosynthetic analysis of compound 3SH is shown in Fig. 7. The C=C alkene of compound 3SH could be generated from the Claisen-Schmidt condensation reaction between 9-oxo-9*H*-xanthene-2-carbaldehyde and 1-(3-mercaptophenyl)ethan-1-one. The oxo-9*H*-xanthene-2-carbaldehyde could be synthesized from 2-hydroxybenzoic acid and 4-hydroxybenzaldehyde through a cyclo-condensation reaction. On the other hand, 1-(3-mercaptophenyl)ethan-1-one could be prepared from benzenethiol and acetyl chloride through a Friedel-Craft acylation reaction. This retrosynthetic analysis demonstrates that compound 3SH could be obtained from four commercially available chemicals through three chemical reactions. We encourage the organic chemists to synthesize compound 3SH and evaluate its anticancer activity in the laboratory in the future.

■ CONCLUSION

We have investigated thirty-seven xanthone-chalcone derivatives with fluoro, chloro, bromo, iodo, cyano, carboxylic acid, nitro, sulfonic acid, methyl, amino, hydroxy, and thiol substituents at ortho, meta, and

para substituents against EGFR receptor through *in silico* studies. From the investigated functional groups, the order of binding energy from the strongest one to the weakest one is as follows: amino < bromo < sulfonic acid < hydrogen < carboxylic acid < fluoro < hydroxyl < nitro < chlorine < cyano < iodo < methyl < thiol. Among the investigated compounds, compound 3SH was found to be the most promising candidate due to its strongest binding energy (-9.71 kcal/mol) and the lowest binding constant (0.08 μ M). The molecular dynamics simulation for 100 ns indicated that a complex structure of EGFR-3SH was stable, as reflected by the Δ RMSD, RMSF, RoG, and SASA parameters. The original and final conformations of the EGFR-3SH complex from the molecular dynamics simulations showed that each chalcone, xanthone, and thiol moieties of compound 3SH interacted well with the key amino acid residues. These amino acid residues are responsible for the physiological function of the EGFR receptor; thus, the observed non-covalent interactions clearly demonstrate the potency of compound 3SH as a novel anticancer agent based on the EGFR inhibition mechanism.

■ ACKNOWLEDGMENTS

The financial support from the Directorate of Research, Technology and Community Service (DRTPM), Ministry of Education, Culture, Research, and Technology (KEMENDIKBUDRISTEK), The Republic of Indonesia through Penelitian Disertasi Doktor (PDD) grant with a contract number of 3102/UN1/DITLIT/Dit-Lit/PT.01.03/2023 was greatly acknowledged. The first author thanks the Indonesia

Endowment Fund for Education (LPDP), Ministry of Finance, The Republic of Indonesia, for the provided scholarship to study as a doctoral student at Universitas Gadjah Mada (2022-2026). The authors also thank Mr. Agus Dwi Ananto and the Austrian-Indonesian Center for Computational Chemistry (AIC), Department of Chemistry, Faculty of Mathematics and Natural Sciences, Universitas Gadjah Mada for providing Yasara and Gaussian09 licenses in this work.

■ AUTHOR CONTRIBUTIONS

Jumina, Harno Dwi Pranowo, and Eti Nurwening Sholikhah conceived and designed the experiments. Yehezkiel Steven Kurniawan, Ervan Yudha, Gerry Nugraha, and Nela Fatmasari conducted the experiment and analyzed the data. Harno Dwi Pranowo contributed materials/analysis instrument. Yehezkiel Steven Kurniawan and Ervan Yudha wrote and revised the manuscript. All authors agreed to the final version of this manuscript.

■ REFERENCES

- [1] Siegel, R.L., Miller, K.D., Fuchs, H.E., and Jemal, A., 2021, Cancer statistics, 2021, *CA-Cancer J. Clin.*, 71 (1), 7–33.
- [2] Pulcini, R., D'Agostino, S., Dolci, M., Bissoli, A., Caporaso, L., and Iarussi, F., 2022, The Impact of COVID-19 on oral cancer diagnosis: A systematic review, *J. Multidiscip. Appl. Nat. Sci.*, 2 (2), 65–69.
- [3] Chopra, B., and Dhingra, A.K., 2021, Natural products: A lead for drug discovery and development, *Phytother. Res.*, 35 (9), 4660–4702.
- [4] Saldívar-González, F.I., Aldas-Bulos, V.D., Medina-Franco, J.L., and Plisson, F., 2022, Natural product drug discovery in the artificial intelligence era, *Chem. Sci.*, 13 (6), 1526–1546.
- [5] Husni, A., Gazali, M., Nurjanah, N., Syafitri, R., Matin, A., and Zuriat, Z., Cytotoxic activity of green seaweed *Halimeda tuna* methanolic extract against lung cancer cells, *J. Multidiscip. Appl. Nat. Sci.*, 10.47352/jmans.2774-3047.172.
- [6] Rasyid, H., Purwono, B., Hofer, T.S., and Pranowo, H.D., 2019, Hydrogen bond stability of quinazoline derivatives compounds in complex against EGFR using molecular dynamics simulation, *Indones. J. Chem.*, 19 (2), 461–469.
- [7] Rasyid, H., Purwono, B., and Pranowo, H.D., 2021, Design of new quinazoline derivative as EGFR (epidermal growth factor receptor) inhibitor through molecular docking and dynamics simulation, *Indones. J. Chem.*, 21 (1), 201–211.
- [8] Ahmeed, N., Erlista, G.P., Raharjo, T.J., Swasono, R.T., and Raharjo, S., 2023, Anticancer activity of venom protein hydrolysis fraction of equatorial spitting cobra (*Naja sumatrana*), *Indones. J. Chem.*, 23 (2), 510–522.
- [9] Hassanpour, S.H., and Dehghani, M., 2017, Review of cancer from perspective of molecular, *J. Cancer Res. Pract.*, 4 (4), 127–129.
- [10] Lee, H.S., Jo, S., Lim, H.S., and Im, W., 2012, Application of binding free energy calculations to prediction of binding modes and affinities of MDM2 and MDMX inhibitors, *J. Chem. Inf. Model.*, 52 (7), 1821–1832.
- [11] Lee, S., Kim, J., Duggirala, K.B., Go, A., Shin, I., Cho, B.C., Choi, G., Chae, C.H., and Lee, K., 2018, Allosteric inhibitor TREA-0236 containing non-hydrolysable quinazoline-4-one for EGFR T790M/C797S mutants inhibition, *Bull. Korean Chem. Soc.*, 39 (7), 895–898.
- [12] Duggirala, K.B., Choe, H., Jeon, B.U., Jung, M.E., Go, A., Lim, B., Park, C., Yoon, J., Chae, C.H., Cho, B.C., Choi, G., and Lee, K., 2019, Identification of TRE-130 as reversible inhibitor of Pan-EGFR mutants while sparing EGFR wild-type activity, *Bull. Korean Chem. Soc.*, 40 (12), 1222–1225.
- [13] Uribe, M.L., Marocco, I., and Yarden, Y., 2021, EGFR in cancer: Signaling mechanisms, drugs, and acquired resistance, *Cancers*, 13 (11), 2748.
- [14] Sudhakar, D.R., Kalaiarasan, P., and Subbarao, N., 2016, Docking and molecular dynamics simulation study of EGFR1 with EGF like peptides to understand molecular interactions, *Mol. BioSyst.*, 12 (6), 1987–1995.
- [15] Stamos, J., Sliwkowski, M.X., and Eigenbrot, C., 2002, Structure of the epidermal growth factor receptor kinase domain alone and in complex with

- a 4-anilinoquinazoline inhibitor, *J. Biol. Chem.*, 277 (48), 46265–46272.
- [16] Kim, D.K., Kim, Y.S., Kim, C.S., and Lee, N.K., 2021, Method for the rapid screening of drug candidates using single-protein tracking in a living cell, *Bull. Korean Chem. Soc.*, 42 (3), 393–397.
- [17] Choe, H., Jeon, B.U., Jung, M.E., Jeon, M.K., Shin, I., Cho, B.C., Choi, G., Chae, C.H., and Lee, K., 2017, Structure-activity relationship study of 2,4-dianilinopyrimidine containing methansulfonamide (TRE-069) as potent and selective epidermal growth factor receptor T790M/C797S mutant inhibitor for anticancer treatment, *Bull. Korean Chem. Soc.*, 38 (11), 1353–1357.
- [18] Sabe, V.T., Ntombela, T., Jhamba, L.A., Maguire, G.E.M., Govender, T., Naicker, T., and Kruger, H.G., 2021, Current trends in computer aided drug design and a highlight of drugs discovered via computational techniques: A review, *Eur. J. Med. Chem.*, 224, 113705.
- [19] Brogi, S., Ramalho, T.C., Kuca, K., Medina-Franco, J.L., and Valko, M., 2020, Editorial: *In silico* methods for drug design and discovery, *Front. Chem.*, 8, 612.
- [20] Kurniawan, Y.S., Indriani, T., Amrulloh, H., Adi, L.C., Imawan, A.C., and Priyanga, K.T.A., 2023, The journey of natural products: From isolation stage to drugs approval in clinical trials, *Bioactivities*, 1 (2), 43–60.
- [21] Pagadala, N.S., Syed, K., and Tuszynski, J., 2017, Software for molecular docking: A review, *Biophys. Rev.*, 9 (2), 91–102.
- [22] Hospital, A., Goñi, J.R., Orozco, M., and Gelpi, J., 2015, Molecular dynamics simulations: Advances and applications, *Adv. Appl. Bioinf. Chem.*, 8, 37–47.
- [23] Pinto, M.M.M., Palmeira, A., Fernandes, C., Resende, D.I.S.P., Sousa, E., Cidade, H., Tiritan, M.E., Correia-da-Silva, M., and Cravo, S., 2021, From natural products to new synthetic small molecules: A journey through the world of xanthenes, *Molecules*, 26 (2), 431.
- [24] Resende, D.I.S.P., Durães, F., Maia, M., Sousa, E., and Pinto, M.M.M., 2020, Recent advances in the synthesis of xanthenes and azaxanthenes, *Org. Chem. Front.*, 7 (9), 3027–3066.
- [25] Wairata, J., Sukandar, E.R., Fadlan, A., Purnomo, A.S., Taher, M., and Ersam, T., 2021, Evaluation of the antioxidant, antidiabetic, and antiplasmodial activities of xanthenes isolated from *Garcinia forbesii* and their *in silico* studies, *Biomedicines*, 9 (10), 1380.
- [26] Cidade, H., Rocha, V., Palmeira, A., Marques, C., Tiritan, M.E., Ferreira, H., Lobo, J.S., Almeida, I.F., Sousa, M.E., and Pinto, M., 2020, *In silico* and *in vitro* antioxidant and cytotoxicity evaluation of oxygenated xanthone derivatives, *Arabian J. Chem.*, 13 (1), 17–26.
- [27] Singh, A., Kaur, N., Sharma, S., and Bedi, P.M.S., 2016, Recent progress in biologically active xanthenes, *J. Chem. Pharm. Res.*, 8 (1), 75–131.
- [28] Kurniawan, Y.S., Priyanga, K.T.A., Jumina, J., Pranowo, H.D., Sholikhah, E.N., Zulkarnain, A.K., Fatimi, H.A., and Julianus, J., 2021, An update on the anticancer activity of xanthone derivatives: A review, *Pharmaceuticals*, 14 (11), 1144.
- [29] Gao, F., Huang, G., and Xiao, J., 2020, Chalcone hybrids as potential anticancer agents: Current development, mechanism of action, and structure-activity relationship, *Med. Res. Rev.*, 40 (5), 2049–2084.
- [30] Rammohan, A., Reddy, J.S., Sravya, G., Rao, C.N., and Zyryanov, G.V., 2020, Chalcone synthesis, properties and medicinal applications: A review, *Environ. Chem. Lett.*, 18 (2), 433–458.
- [31] Salehi, B., Quispe, C., Chamkhi, I., El Omari, N., Balahbib, A., Sharifi-Rad, J., Bouyahya, A., Akram, M., Iqbal, M., Docea, A.O., Caruntu, C., Leyva-Gómez, G., Dey, A., Martorell, M., Calina, D., López, V., and Les, F., 2021, Pharmacological properties of chalcones: A review of preclinical including molecular mechanisms and clinical evidence, *Front. Pharmacol.*, 11, 592654.
- [32] Leite, F.F., de Sousa, N.F., de Oliveira, B.H.M., Duarte, G.D., Ferreira, M.D.L., Scotti, M.T., Filho, J.M.B., Rodrigues, L.C., de Moura, R.O., Mendonça-Junior, F.J.B., and Scotti, L., 2023, Anticancer activity of chalcones and its derivatives:

- Review and *in silico* studies, *Molecules*, 28 (10), 4009.
- [33] Anwar, C., Prasetyo, Y.D., Matsjeh, S., Haryadi, W., Sholikhah, E.N., and Nendrowati, N., 2018, Synthesis of chalcone derivatives and their *in vitro* anticancer test against breast (T47D) and colon (WiDr) cancer cell line, *Indones. J. Chem.*, 18 (1), 102–107.
- [34] Suma, A.A.T., Wahyuningsih, T.D., and Mustofa, M., 2019, Efficient synthesis of chloro chalcones under ultrasound irradiation, their anticancer activities and molecular docking studies, *Rasayan J. Chem.*, 12 (2), 502–510.
- [35] Li, P.H., Jiang, H., Zhang, W.J., Li, Y.L., Zhao, M.C., Zhou, W., Zhang, L.Y., Tang, Y.D., Dong, C.Z., Huang, Z.S., Chen, H.X., and Du, Z.Y., 2018, Synthesis of carbazole derivatives containing chalcone analogs as non-intercalative topoisomerase II catalytic inhibitors and apoptosis inducers, *Eur. J. Med. Chem.*, 145, 498–510.
- [36] Zhou, W., Zhang, W., Peng, Y., Jiang, Z.H., Zhang, L., and Du, Z., 2020, Design, synthesis and anti-tumor activity of novel benzimidazole-chalcone hybrids as non-intercalative topoisomerase II catalytic inhibitors, *Molecules*, 25 (14), 3180.
- [37] Liu, J., Zhou, F., Zhang, L., Wang, H., Zhang, J., Zhang, C., Jiang, Z., Li, Y., Liu, Z., and Chen, H., 2018, DMXAA-pyranoanthone hybrids enhance inhibition activities against human cancer cells with multi-target functions, *Eur. J. Med. Chem.*, 143, 1768–1778.
- [38] Georgakopoulos, A., Kalampaliki, A.D., Gioti, K., Hamdoun, S., Giannopoulou, A.F., Efferth, T., Stravopodis, D.J., Tenta, R., Marakos, P., Pouli, N., and Kostakis, I.K., 2020, Synthesis of novel xanthone and acridone carboxamides with potent antiproliferative activities, *Arabian J. Chem.*, 13 (11), 7953–7969.
- [39] Iresha, M.R., Jumina, J., Pranowo, H.D., Sholikhah, E.N., and Hermawan, F., 2022, Synthesis, cytotoxicity evaluation and molecular docking studies of xanthyl-cinnamate derivatives as potential anticancer agents, *Indones. J. Chem.*, 22 (5), 1407–1417.
- [40] Fatmasari, N., Kurniawan, Y.S., Jumina, J., Anwar, C., Priastomo, Y., Pranowo, H.D., Zulkarnain, A.K., and Sholikhah, E.N., 2022, Synthesis and *in vitro* assay of hydroxyxanthenes as antioxidant and anticancer agents, *Sci. Rep.*, 12 (1), 1535.
- [41] Meng, X.Y., Zhang, H.X., Mezei, M., and Cui, M., 2011, Molecular docking: A powerful approach for structure-based drug discovery, *Curr. Comput.-Aided Drug Des.*, 7 (2), 146–157.
- [42] Chabaan, I., Hafez, H., AlZaim, I., Tannous, C., Ragab, H., Hazzaa, A., Ketat, S., Ghoneim, A., Katary, M., Abd-Alhaseeb, M.M., Zouein, F.A., Albohy, A., Amer, A.N., El-Yazbi, A.F., and Belal, A.S.F., 2021, Transforming iodoquinol into broad spectrum anti-tumor leads: Repurposing to modulate redox homeostasis, *Bioorg. Chem.*, 113, 105035.
- [43] Sun, J., Wei, Q., Zhou, Y., Wang, J., Liu, Q., and Xu, H., 2017, A systematic analysis of FDA-approved anticancer drugs, *BMC Syst. Biol.*, 11 (5), 87.
- [44] Saladi, J.S.C., Nangi, G.B.S., Chavakula, R., Karumanchi, K., and Bonige, K.B., 2023, Identification and synthesis of potential process-related impurities of trametinib: An anti-cancer drug, *Chem. Pap.*, 77 (3), 1759–1763.
- [45] Dai, Z., and Wang, Z., 2020, Photoactivable platinum-based anticancer drugs: Mode of photoactivation and mechanism of action, *Molecules*, 25 (21), 5167.
- [46] Rappaport, J., 2017, Changes in dietary iodine explains increasing incidence of breast cancer with distant involvement in young women, *J. Cancer*, 8 (2), 174–177.
- [47] Zhang, D., Xu, X., Li, J., Yang, X., Sun, J., Wu, Y., and Qiao, H., 2019, High iodine effects on the proliferation, apoptosis, and migration of papillary thyroid carcinoma cells as a result of autophagy induced by BRAF kinase, *Biomed. Pharmacother.*, 120, 109476.
- [48] Darbandi, A., Gavahi, M., Shirani Bidabadi, E., Kadhim, M.M., Naghsh, N., Canli, G., and Ahmed, O.S., 2022, Complexation of mercaptopurine anticancer drug with an iron-doped fullerene cage: DFT assessments of drug delivery approach, *Phys. Lett. A*, 448, 128318.

- [49] Munshi, P.N., Lubin, M., and Bertino, J.R., 2014, 6-Thioguanine: A drug with unrealized potential for cancer therapy, *Oncologist*, 19 (7), 760–765.
- [50] Chen, X., Jia, F., Huang, Y., Jin, Q., and Ji, J., 2022, Cancer-associated fibroblast-targeted delivery of captopril to overcome penetration obstacles for enhanced pancreatic cancer therapy, *ACS Appl. Bio Mater.*, 5 (7), 3544–3553.
- [51] Shahzadi, I., Zahoor, A.F., Tüzün, B., Mansha, A., Anjum, M.N., Rasul, A., Irfan, A., Kotwica-Mojzycz, K., and Mojzycz, M., 2022, Repositioning of acefylline as anti-cancer drug: Synthesis, anticancer and computational studies of azomethines derived from acefylline tethered 4-amino-3-mercaptop-1,2,4-triazole, *PLoS One*, 17 (12), e0278027.
- [52] Ptaff, A.R., Beltz, J., King, E., and Ercal, N., 2020, Medicinal thiols: Current status and new perspectives, *Mini-Rev. Med. Chem.*, 20 (6), 513–529.
- [53] Dalzoppo, D., Di Paolo, V., Calderan, L., Pasut, G., Rosato, A., Caccuri, A.M., and Quintieri, L., 2017, Thiol-activated anticancer agents: The state of the art, *Anti-Cancer Agents Med. Chem.*, 17 (1), 4–20.
- [54] Sun, S., Oliveira, B.L., Jiménez-Osés, G., and Bernardes, G.J.L., 2018, Radical-mediated thiol-ene strategy: Photoactivation of thiol-containing drugs in cancer cells, *Angew. Chem., Int. Ed.*, 57 (48), 15832–15835.
- [55] Kurniawan, Y.S., Fatmasari, N., Jumina, J., Pranowo, H.D., and Sholikhah, E.N., 2023, Evaluation of the anticancer activity of hydroxyxanthenes against human liver carcinoma cell line, *J. Multidiscip. Appl. Nat. Sci.*, 10.47352/jmans.2774-3047.165.
- [56] Choowongkamon, K., Sawatdichaikul, O., Songtawee, N., and Limtrakul, K., 2010, Receptor-based virtual screening of EGFR kinase inhibitors from the NCI diversity database, *Molecules*, 15 (6), 4041–4054.
- [57] Almalki, F.A., Shawky, A.M., Abdalla, A.N., and Gouda, A.M., 2021, Icotinib, almonertinib, and olmutinib: A 2D similarity/docking-based study to predict the potential binding modes and interactions into EGFR, *Molecules*, 26 (21), 6423.
- [58] Balasubramanian, P.K., Lee, Y., and Kim, Y., 2019, Identification of ligand-binding hotspot residues of CDK4 using molecular docking and molecular dynamics simulation, *Bull. Korean Chem. Soc.*, 40 (10), 1025–1032.
- [59] Nugraha, G., Pranowo, H.D., Mudasir, M., and Istyastono, E.P., 2022, Virtual target construction for discovery of human histamine H4 receptor ligands employing a structure-based virtual screening approach, *Int. J. Appl. Pharm.*, 14 (4), 213–218.
- [60] Istyastono, E.P., and Riswanto, F.D.O., 2022, Molecular dynamics simulations of the caffeic acid interactions to dipeptidyl peptidase IV, *Int. J. Appl. Pharm.*, 14 (4), 274–278.